www.amlett.com, www.vbripress.com/aml, DOI: 10.5185/amlett.2015.5715 Published online by the VBRI press in 2015

Ag nano-composite glasses synthesized by swift heavy ion irradiation

Ranjana S. Varma[1*], D.C. Kothari[1], S. Santra[2], R.G. Thomas[2], R. Tewari[3], S. Neogy[3], C.S. Suchand Sandeep[4], Reji Philip[4], D. Kanjilal[5]

[1]*Department of Physics & National Centre for Nanosciences and Nanotechnology, University of Mumbai, Vidyanagari, Santacruz East,Mumbai 400 098, India*
[2]*Nuclear Physics Division, Bhabha Atomic Research Centre, Trombay, Mumbai 400 085, India*
[3]*Materials Science Division, Bhabha Atomic Research Centre, Mumbai 400 085, India*
[4]*Raman Research Institute, Sadashiva Nagar, Bangalore 560 080, India*
[5]*Inter-University Accelerator Centre, Aruna Asaf Ali Marg, Post Box: 10502, New Delhi 110067, India*

[*]Corresponding author. Tel: (+91) 9821216711; E-mail: ranju16@gmail.com

Received: 20 October 2014, Revised: 17 December 2014 and Accepted: 24 December 2014

ABSTRACT

In the present work, we have used swift heavy ions (SHI) irradiation and post irradiation annealing to synthesize Ag nanoparticles in fused silica. Fused silica samples deposited with 15 nm of Ag film were irradiated using SHI beam of 120 MeV Ag^{9+} ions at different fluences and post irradiation annealing was done at 500 °C in air for 30 min. The samples were characterized using UV-vis absorption spectroscopy, Rutherford Backscattering Spectrometry (RBS), GAXRD, Transmission Electron Microscopy (TEM), and open aperture z-scan measurements. The signature of Ag nanoparticles was observed in optical absorption spectra and the average size of the Ag nanoparticles was estimated using Mie's theory. The size of the nanoparticles (~3 nm) was also confirmed from the GAXRD and TEM measurements. RBS results for Ag/SiO_2 irradiated with the fluence of 5 x10^{13} ions/cm^2 shows the decrease in slope at the interface of the Ag profile, indicating a partial mixing at a fluence of 5 x 10^{13} ions/cm^2. Open aperture z-scan measurement of Ag/SiO_2 SHI irradiated sample after annealing shows a saturation behavior, indicating that the sample is optically non-linear. The sample shows saturation behavior but does not show optical limiting behavior, which indicates that the size and number density of nanoparticles are low. The ability to control the particle size using ion beam technique as a function of fluence and observed nonlinearity results provide concrete evidence that Ag nano composite glasses can be used in nonlinear and optical limiting application. Copyright © 2015 VBRI press.

Keywords: Ag nanoparticles; swift heavy ion irradiation; RBS, TEM; z-scan.

Ranjana Santosh Varma is working as Women Scientist-A, (DST project) in the Department of Physics, University of Mumbai, India. Her current research interests include synthesis and characterization of nanocomposite materials; ions beam techniques and photocatalysis. She received her PhD degree in Physics in 2009 from University of Mumbai, India.

Introduction

Over the last decade, there has been an ever increasing interest in metal nanoparticles as they are considered candidates for many technological applications such as biosensor, plasmonic devices, optical limiters, Surface Enhanced Raman Scattering (SERS) and plasmonic chain waveguides **[1-5]**. Metal Nanoparticle Composite Glasses (MNCG), exhibit an enhanced third order optical Kerr susceptibility ($\chi^{(3)}$) in the picosecond regime which can be used to realize all-optical switching devices **[1, 6]**. Precise control of particle sizes during the synthesis of metal nanoparticles in a glass matrix is of prime importance as the optoelectronic properties of nanoparticles depend primarily on nanoparticles size, shape, distribution, interparticle distances and variations in size degrade the performance **[7, 8]**. In this context, ion beam based techniques to create and modify shape and arrangement of the metal particles are of great interest since they provide a very powerful and flexible tool to control and optimize the linear and nonlinear optical properties of these materials **[8, 9]**. Ion beam offers great flexibility in the nanoparticle formation by control of the process parameters, considerable freedom from thermodynamic limitations and extreme chemical purity. Additionally, it enables dense packing of nanoclusters, and is compatible with the integrated circuit technology **[10]**.

High-energy heavy ions with velocities comparable to or higher than the orbital electron velocity are referred to as swift heavy ions (SHI). At such energies (a few tens of keV/nucleon and higher) SHI lose their energy in the target mainly via inelastic collisions leading to the excitation of the target electrons. Swift heavy ion beam mixing is strongly related to nuclear track formation **[11]**. Such latent nuclear tracks (i.e. amorphous cylindrical region of some nm in diameter) were often found in insulating materials, while metals seem to be much less sensitive to electronic energy deposition **[12, 13]**. Track formation occurs only if material-dependent threshold S_{et} of the electronic stopping is exceeded (Typical values reported are 1.8 keV/nm, 67 keV/nm for SiO_2 & Ag respectively) **[13, 14]**.

However, there are few reports for mixing across the interfaces of metallic bilayers systems due to inelastic thermal spike, consisting of one S_e-sensitive and another S_e-insensitive metal, by heat exchange along the ion track **[15-18]**. In both the cases, the melting temperature of S_e-insensitive material was lower than that of S_e-sensitive material. Eventhough bulk metal is insensitive to SHI irradiation; it was found that mixing increases with fluence and with the electronic energy loss **[17]**. At the interface, the insensitive material behavior could be modified by the sensitive material under heavy ion irradiation, leading to the appearance of a molten phase in some layers of insensitive material. Therefore, the intermixing at the interfaces of SHI irradiated bilayers is usually attributed to interdiffusion in the molten ion tracks, although mixing is lower than the case where both materials are sensitive to S_e **[17]**.

These studies motivated us to study SHI induced mixing in a metal/ceramic (Ag/SiO_2) system where the S_e-insensitive material has a lower melting temperature than that of the corresponding S_e-sensitive material. This would help to check for the applicability of the hypothesis of heat exchange across the interface along the ion track under the present configuration (Ag/SiO_2 bilayer system). In this article, we explore a route to form Ag nanoparticles in fused silica glasses using ion beam mixing of a thin Ag layer deposited on the fused silica glass substrates. The effect of post-irradiation thermal annealing is manifested by the growth of these embedded Ag particles. We also, have investigated the nonlinear optical transmission of these samples using pulsed laser (pulse width 5 ns) of 532 nm wavelength.

Experimental

Materials

High-purity fused silica glass plates, of size 10 mm x 10 mm x 1.5 mm, were chosen as substrates. The glass slides were ultrasonically cleaned in distilled water and acetone, for 15 minutes.

Method

Silver films of 15 nm thickness were deposited on the fused silica substrates using vacuum evaporation at a pressure of 3×10^{-5} mbar. The coated samples were then irradiated at fluence of 5×10^{12} and 5×10^{13} ions/cm^2 using 120 MeV Ag^{9+} beam, provided by the pelletron accelerator of the IUAC, Delhi. After irradiation, the samples were annealed at 500 °C in air for 30 min, to promote nanoparticle growth/formation. 4 MeV proton beam from Folded Tandem Ion Accelerator (FOTIA) at BARC, Mumbai, was used for Rutherford backscattering (RBS) measurements at backscattering angle of 160°. The RBS data was fitted with Rutherford Universal Manipulation Program (RUMP) code **[19]**. Optical absorption studies were carried out using Shimadzu 3600 UV-Vis-NIR spectrometer. GAXRD was done on X'pert-Pan Analytical XRD machine having an X-ray wavelength of 0.154 nm (Cu-K_α source). The samples for transmission electron microscopy (TEM) were prepared by cutting 3 mm diameter discs from the irradiated area with a slurry drill, mechanical grinding of the disc from the backside to a thickness of about 20 μm was carried out. The final thinning to the electron transparency was achieved by planar back thinning by Ar ion milling (IV4: Technoorg Linda, High Energy Ion Polishing System), operating at 4 kV. Here milling was started with high energy and slowed to the lower energy as the perforation approached to avoid the physical damage to the sample. The prepared samples were examined in a Transmission electron microscopy (TEM) using JEOL 200 FX microscope. Optical nonlinearity in the prepared samples was determined using the open aperture z scan method. The measurements of the nonlinear optical transmission at 532 nm were made with an Nd:YAG laser (pulse width = 5 ns).

Results and discussion

The electronic energy loss (S_e) and nuclear energy loss (S_n) in SiO_2 at the Ag/SiO_2 interface for 120 MeV Ag^{9+} ions estimated using the SRIM code are 8.63 keV/nm and 0.042 keV/nm respectively. The S_e values clearly exceeded the 1 keV/nm threshold value for track formation in fused silica (SiO_2); tracks of 3 nm radius are reported to be formed for S_e = 8 keV/nm **[20]**. Thus ion energies were sufficient to produce tracks of radii greater than 3 nm in fused silica **[21]**. Also, from S_e and S_n values, the value of S_n for 120 MeV Ag^{9+} ions in SiO_2 near the Ag/SiO_2 interface is two orders of magnitude lower than the corresponding S_e value and the dominant process during nanoparticle formation in SiO_2 is electronic energy loss.

Ion Beam Mixing (IBM) is a process in which the atoms of two different atomic species across an interface mingle together under the influence of the passage of ion beam. Mixing achieved at low energies (keV) is referred to low energy ion beam mixing with the dominance of elastic collisions followed by nuclear energy loss while the mixing at higher energies (MeV) is referred to swift heavy ion induced mixing with the major contribution of inelastic collisions followed by electronic energy loss **[16-18]**. Ion beam effect on the materials depends on the ion energy, fluence and ion species. The interaction of the ion with material is the deciding factor in the ion beam induced material modification. Depending on the energy density, the melting point of the materials can be exceeded in a region around the ion track **[17 - 18]**.

Fig. 1 shows the RBS spectra of Ag/SiO_2 ion beam mixed sample at different fluences by SHI irradiation in comparison with the as deposited films. The peak, due to metal atoms, shows reduction in height and decrease in

slope of the rising part of Gaussian (on the interface side). The decrease in slope indicates partial ion beam mixing at the interface. The decrease in height indicates decrease in number of metal atoms due to sputtering. The sputtering yield of two to three orders of magnitude higher than that expected for bulk Ag was observed by Singh et al. **[21]** from SHI irradiation of thin Ag film by 120 MeV Ag ions. The observed modifications were found at much below the predicted threshold values of defect production for Ag thin film. This may be due to small thickness of the film, which may decrease mobility of the conduction electrons. This mobility change can be due to interface scattering resulting in confinement of the deposited energy to a smaller region thus raising its temperature and enhancing the interdiffusion. During SHI irradiation the electronic excitation and electron–phonon and phonon–phonon coupling processes are expected to produce defects due to the atomic rearrangements and thereby enhance mixing at interfaces **[18]**.

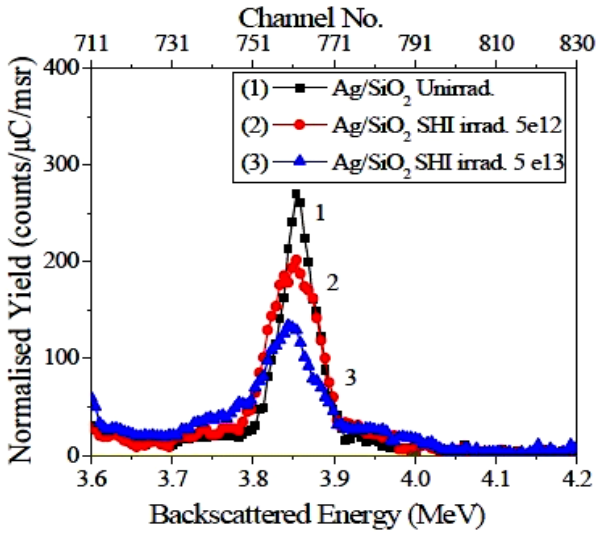

Fig. 1. RBS spectra of Ag/SiO_2 samples (1) unirradiated, and irradiated with 120 MeV Ag^{9+} ion irradiations at the different fluencies: (2) 5 x 10^{12} ions/cm^2 (3) 5 x 10^{13} ions/cm^2.

The greater the electron–phonon coupling constant the more will be the energy transferred to the lattice causing more vibrations of the atoms. In the sample each impinging ion produces a track and their number and size increases with increasing energy due to overlapping and accumulation of individual tracks. In the framework of the thermal spike model, the excited electrons are in a thermodynamical equilibrium in some 10^{-15} s via electron–electron interactions and release their energy to lattice atoms via electron–phonon coupling in 10^{-13}–10^{-10} s. This generates a transient thermal spike (≥1000 K, depending on the ion and the solid) in the lattice subsystem for time duration of a fraction of a pico second to about 100 ps **[12]**. The temperature spike, and hence the electronic sputtering, depends strongly on the electron phonon (e–p) coupling strength, g, which is dependent on the mean diffusion length, λ of the excited electrons by the relation **[12]**.

$$g = \frac{D_e(T_e)C_e(T_e)}{\lambda^2} \qquad (1)$$

where, $D_e(T_e)$ is the spatial energy distribution, $C_e(T_e)$ the electronic specific heat of the system & T_e: temperature of electronic subsystem. In any particular system, one of the most salient factors that decide the lattice temperature developed is λ. The increase in thermal energy density in the lattice due to the restricted motion of excited electrons is discussed in literature **[21]**. This enhances the e–p coupling strength according to Eq. (1) which is the increased ability to transfer the energy to the lattice subsystem. Hence, from the basic heat diffusion equations of thermal spike model **[11-13]** we can say that the temperature spike generated in the lattice subsystem of the thin film is high. The thermal energy in the lattice dissipates less efficiently in thinner film, due to smaller available cross sectional area (Fick's law). Therefore, the spike temperature will prevail for a longer duration in thinner film. However, higher temperature spike and sustaining the spike temperature for a longer duration causes higher sputtering of the thinner films. Also, ion irradiation leads to the formation of Ag nanoparticles in the SiO_2 matrix (as revealed from absorption spectroscopy for higher fluence as shown in **Fig. 2** due to partial beam mixing at the interface which is revealed from the RBS spectrum. This is due to increase in electron phonon coupling at the thin film interface which leads to the heat exchange across the interface in few layers of the film along the ion track under the present configuration (Ag/SiO_2 bilayer system).

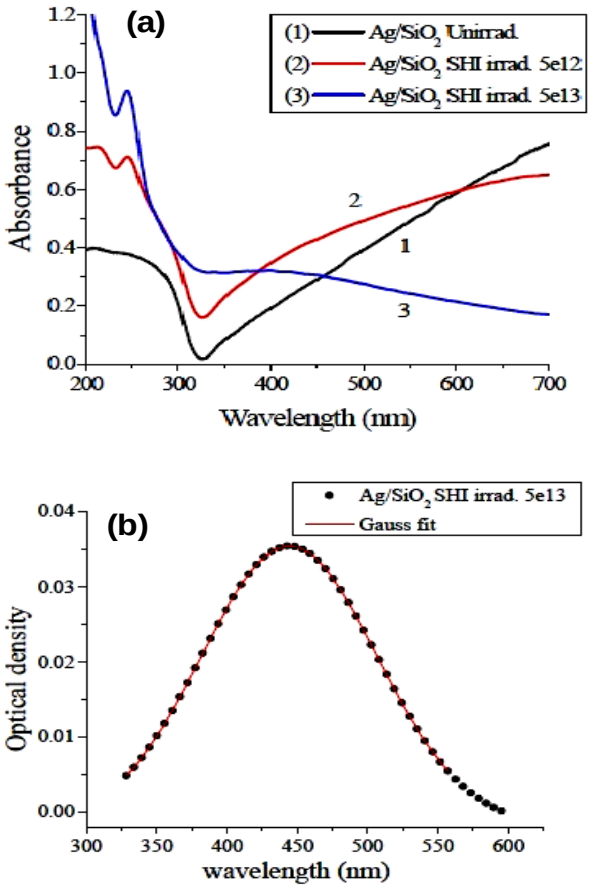

Fig. 2. (a) UV–vis absorption spectra of Ag/SiO_2 samples (1) unirradiated, and irradiated with 120 MeV Ag^{9+} ion irradiations at the different fluences (2) 5 x 10^{12} ions/cm^2 (3) 5 x 10^{13} ions/cm^2 and (b) Optical density of Ag/SiO_2 sample after irradiation with 120 MeV Ag^{9+} ion irradiations at the fluences of 5 x 10^{13}ions/cm^2.

Fig. 2 (a) shows the UV–vis absorption spectra for Ag/SiO_2 samples before and after 120 MeV Ag^{9+}, irradiation as a function of the ion fluence. The spectra of the irradiated samples show two peaks at 215 and 245 nm arising from the E' and B_2 defect centers created in the SiO_2 substrates **[14]**. With the increase in fluence the absorption of this defect peak intensity increases without changing the peak position implying the increase in defect concentration with fluence. Transmission window seen in **Fig. 2 (a)** at 325 nm is attributed to semitransparent film of Ag displaying its characteristic color (yellow). **Fig. 2 (b)** shows the data for Ag/SiO_2 irradiated samples at 5×10^{13} ions/cm^2 fluence after baseline correction. **Fig. 2 (b)** also shows a Gaussian fit to the experimental data. The average size of the Ag nanoparticles was calculated using the Mie formula [22] from **Fig. 2 (b)** which is 1.1 nm; given in **Table 1**.

Table 1. SPR peak position, FWHM, area of the absorption peaks and radius of the Ag nanoparticles obtained after irradiation of Ag/SiO_2 at different fluences followed by 900 °C annealing for 30 min. in air.

Sample	SPR peak position (lspr) nm	FWHM nm	Area under the SPR peak	Particle radius nm
Ag/SiO_2 irrad 5e13	444.36	147.22	5.84	1.1
Ag/SiO_2 irrad 5e12 annealed	431.44	124.67	26.40	1.4
Ag/SiO_2 irrad 5e13 annealed	407.22	34.71	8.23	3.01

For the irradiated samples, when sufficient thermal energy is supplied to the system during post irradiation annealing, atomic mobility across the interface is enhanced due to SHI induced defects. **Fig. 3 (a)** shows the annealing effect (500 °C in air for 30 min) for samples SHI irradiated at two fluences of 5×10^{12} ions/cm^2 and 5×10^{13} ions/cm^2 and **Fig. 3 (b)** shows the data for Ag/SiO_2 irradiated samples at different fluences followed by annealing after baseline correction. **Fig. 3 (b)** also shows a Gaussian fit to the experimental data.

The average size of the Ag nanoparticles was calculated using the Mie formula **[22]** from **Fig. 3 (b)** is given in **Table 1**. Radius of the Ag nanoparticles increases with the fluence after annealing at fixed temperature of 500 °C. Also, the FWHM values decrease indicating that with the increase in fluence after annealing more uniform Ag nanoparticles are formed.

Fig. 4 shows the GAXRD plots of the Ag/SiO_2 SHI irradiated sample at fluencies of 5×10^{13} ions/cm^2 followed by annealing at 500 °C. The diffraction peaks due to Ag (111) and Ag (200) planes are observed at 2θ = 38.2 and 44.3. The peaks are broad as the particle size is small. The size of the Ag nanoparticles is calculated using the Scherrer formula which is 3.15 nm.

Fig. 5 shows the TEM image and the electron diffraction micrograph taken from the same region, of Ag/SiO_2 SHI irradiated sample at a fluence of 5×10^{13} ions/cm^2 followed by annealing at 500 °C. The average radius of Ag nanoparticle obtained from TEM is 3.2 nm which correlates well with the size obtained from the GAXRD and Mie fit to the SPR peak in UV–vis absorption spectra. The Ag/SiO_2 SHI irradiated sample at high fluence contains nanoparticles of approximately 1 nm radius, and the associated SPR is relatively weak and broad. When this sample is annealed to higher temperatures of 500 °C, the clusters grow to a larger size showing enhanced SPR and absorption.

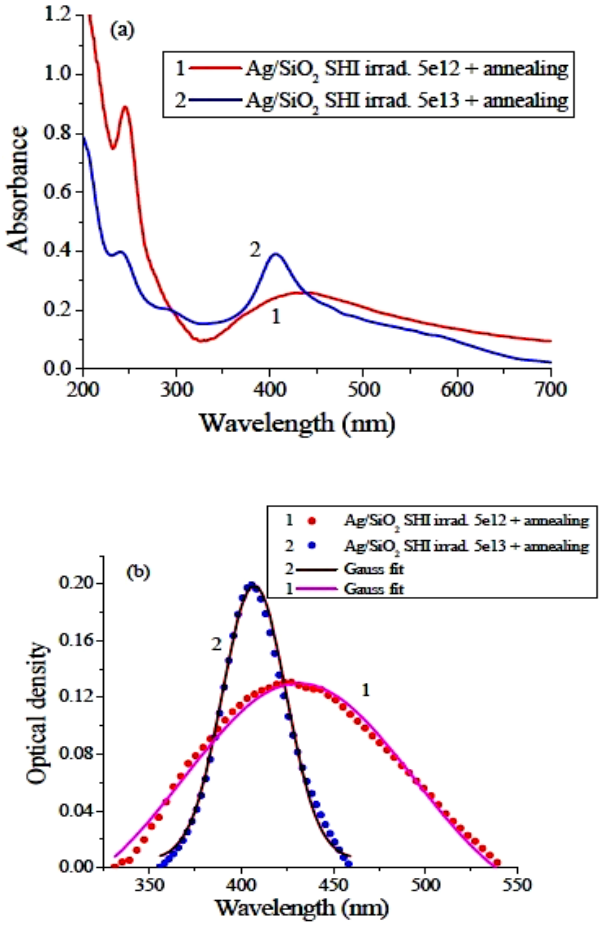

Fig. 3. (a) UV–vis absorption spectra of Ag/SiO_2 samples irradiated with 120 MeV Ag^{9+} ion irradiations at the different fluences (1) 5×10^{12} ions/cm^2, and (2) 5×10^{13} ions/cm^2 followed by annealing at 500 °C in air for 30 min. and (b) Optical density of Ag/SiO_2 samples irradiated with 120 MeV Ag^{9+} ion irradiations at the different fluencies (1) 5×10^{12} ions/cm^2 (2) 5×10^{13} ions/cm^2 followed by annealing at 500 °C in air for 30 min.

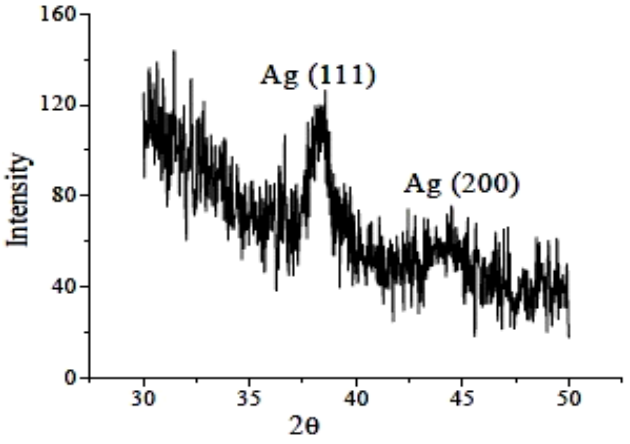

Fig. 4. GAXRD spectra for Ag/SiO_2 sample SHI irradiated with 5×10^{13} ion/cm^2 followed by annealing at 500 °C.

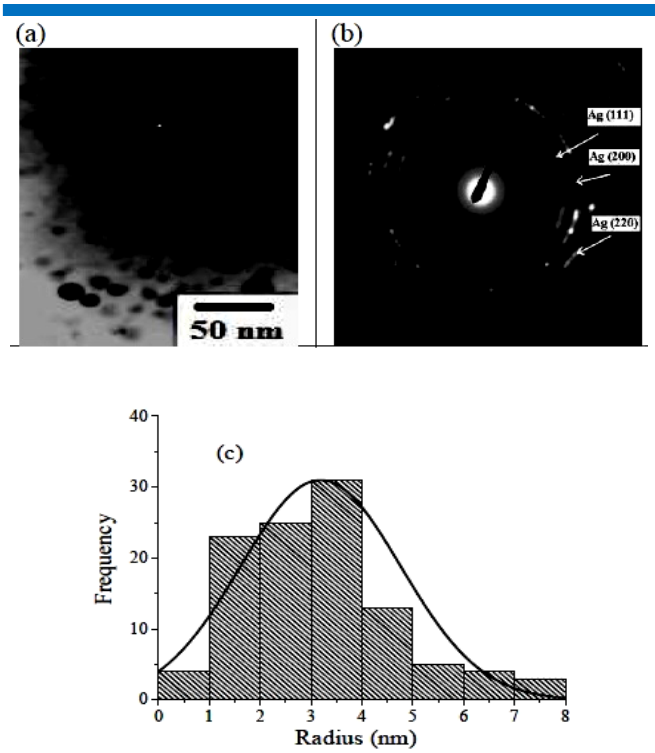

Fig. 5. (a) TEM micrograph showing the presence particles in Ag/SiO_2 sample SHI irradiated with 5 x 10^{13} ions/cm^2 followed by annealing at 500 °C, (b) Diffraction micrograph in which the rings for Ag (1 1 1), (2 0 0) & (2 2 0) planes shown (c) Frequency distribution of the radius of nanoparticles seen in the TEM image as seen in Fig. 5 (a).

Fig. 6 shows the results of open-aperture *z*-scan at 532 nm laser (5 ns) energy of 50 μJ for Ag/SiO_2 SHI irradiated sample at fluence, of 5 x10^{13} ions/cm^{2}after annealing at 500 °C. Nonlinearity is not observed for Ag/SiO_2 SHI irradiated sample at a fluence of 5 x 10^{12} ions/cm^2 before annealing, in which no nanoparticles were observed as seen in a absorption spectroscopy (**Fig. 2**). Fused silica glass without any treatment did not show any nonlinearity (not shown here) and hence we can conclude that the origin of the optical nonlinearity in all the investigated samples is due to the presence of metal nanoparticles only. The result shows the saturation behavior. Nonlinearity will be enhanced when excited near the SPR, due to the local field enhancement. If metal nanoparticles of dielectric constant ε_m are distributed uniformly and randomly in the dielectric host having a dielectric constant ε_d, the local field is given by Eqn (2),

$$E_l = \frac{3\varepsilon_d}{\varepsilon_m + 2\varepsilon_d} E_0 \qquad (2)$$

where, E_0 is the applied optical field. Near the SPR $\varepsilon_m + 2\varepsilon_d$ is minimum, so that E_l is a maximum. The corresponding nonlinear polarization is given by Eqn (3),

$$P_{NLS} = 3p\left(\frac{3\varepsilon_d}{\varepsilon_m + 2\varepsilon_d}\right)^4 \chi_m^{(3)} E_0^3 \qquad (3)$$

which scales as fourth power of the local field factor **[23, 24]**. It is very clear that only SHI irradiated and Ag/SiO_2 SHI irradiated at 5 x 10^{12} ions/cm^2 followed by annealing samples does not show nonlinear absorption (NLA) but the Ag/SiO_2 SHI irradiated sample at 5 x 10^{13} ions/cm^2 shows NLA of a saturable absorption nature (**Fig. 6**). The obtained NLA is fitted numerically to the propagation equation describing the saturable absorption process **[24]** given by,

$$\frac{dI}{dz} = -\left[\frac{\alpha_0}{1 + I/I_s}\right] I$$

where, α_0 is the linear absorption coefficient, I is the incident intensity, I_s is the saturation intensity and z is the propagation distance. The value of the saturation intensity obtained from the numerical fit to the data is 3.3 x 10^{13} W/m^2.

$$T = \left((1-R)^2 \exp(-\alpha_0 L)/\sqrt{\pi} q_0\right) \int_{-\infty}^{+\infty} \ln\left[1 + q_0 \exp(-t^2)\right] dt \qquad (4)$$

where, $q_0 = \beta(1-R) I_0 L_{eff}$ and $L_{eff} = (1 - e^{-\alpha_0 L})/\alpha_0$

here T is the net transmission of the samples, L and R are the sample length and surface reflectivity respectively, α_0 is the linear absorption coefficient, I_0 is the on-axis peak intensity, and β is the two-photon absorption coefficient. The value of two photon absorption coefficient β calculated from numerical fits to the experimental data is 3.3 x 10^{13} W/m^2.

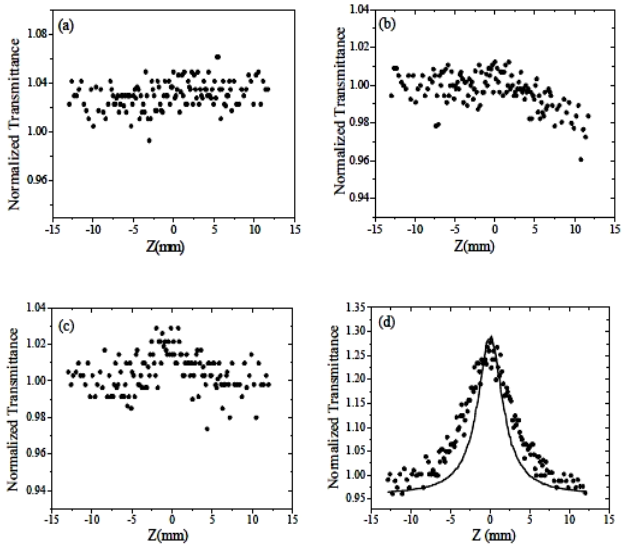

Fig. 6. Open aperture z-scan plots for Ag/SiO_2 SHI irradiated sample (a) at a fluence of 5 x 10^{12} ions/cm^2 (b) at a fluence of 5 x 10^{13} ions/cm^2 (c) at a fluence of 5 x 10^{12} ions/cm^2 followed by annealing at 500 °C and (d) at a fluence of 5 x 10^{13} ions/cm^2 followed by annealing at 500 °C. (Line through solid circles representing the experimental data is a saturable absorption fit to the experimental data).

Conclusion

RBS results for Ag/SiO_2 irradiated with the fluence of 5 x10^{13} ions/cm^2 shows the decrease in slope at the interface of the Ag profile, indicating a partial mixing. The optical study shows that at high fluence of

5 x 10^{13} ions/cm^2 used in the present work nanoparticle formation in the fused silica glass matrix is observed & post irradiation annealing result in growth of the nanopartciles. Open aperture z-scan measurement of SHI irradiated Ag/SiO_2 sample after annealing shows a saturation behavior, indicating that the sample is optically non-linear. The sample shows saturation behavior but does not show optical limiting behavior, which indicates that the size and number density of nanoparticles are low. The observed saturation peak in z-scan result indicates that the optical nonlinearity is enhanced due to nanoparticle formation. The control over the particle size as a function of SHI ion beam technique and observed nonlinearity results provide concrete evidence that Ag nano composite glasses can be used in nonlinear and optical limiting application.

Acknowledgements

This work was supported by the Inter-University Accelerator Centre, New Delhi. The authors are indebted to Nilesh Kulkarni (TIFR, Mumbai) for doing the GAXRD measurements. The authors are indebted to Pelletron group at IUAC, New Delhi for assistance during the Ag-ion irradiations and NPD group from BARC, Mumbai for assistance during the RBS experiments at BARC.

Reference

1. Lal, S.; Link, S.; Halas, N.J.; *Nature Photonics*, **2007**, *1*, 641. **DOI:** 10.1038/nphoton.2007.223
2. Udayabhaskar, R.; Karthikeyan, B.; Ollakkan, M.S.; Mangalaraja, R.V; Baesso, M.L.; *Chem. Phys. Lett.*, **2014**, *593*, 1. **DOI:** 10.1016/j.cplett.2013.12.058
3. Homola, J.; *Chem. Rev.*, **2008**, *108(2)*, 462. **DOI:** 10.1021/cr068107d
4. Fan, M.; Andrade, G.F.S.; Brolo, A.G.; *Analytical Chimica Acta* **2011**, *693(1)*, 7. **DOI:** 10.1016/j.aca.2011.03.002
5. Brunelti, B.G.; Cartechini. Li.; Miliani, C.; Sagamellotti, A.; "Metal Nanoparticles in Glass: Lustre, in Modern Methods for Analysing Archaeological & Historical Glass, (Ed., Janssen, K.), John Wiley & Sons Ltd, Oxford, UK.; **2013**. **DOI:** 10.1002/9781118314234.ch28
6. Ozbay, E.; *Science*, **2006**, *311(5758)*, 189. **DOI:** 10.1126/science.1114849
7. Ghosh, S.K.; Pal, T.; *Chem. Rev.*, **2007**,*107*, 4797. **DOI:** 10.1021/cr0680282
8. Sato, R.; Chnuma, M.; Oyoshi, K.; Takeda, Y.; *Phys Rev B.*, **2014**, *90*, 125417. **DOI:** 10.1103/PhysRevB90.125417
9. Cattaruzza, E.; Battaglin, G.; Calvelli, P.; Gonella, F.; Mattei, G.; Maurizio, C.; Mazzoldi P.; Padovani, S.; Polloni R.; Sada, C.; Scremin, B.F.; Acapito, F.D.; *Composites Science and technology*, **2003**, *63 (8)*, 1203. **DOI:** 10.1016/S0266-3538(03)00079-4
10. Dhara, S.; *Critical Reviews in Solid State and Materials Sciences*, **2007**, *32*, 1. **DOI:** 10.1080/10408430601187624
11. Pivin, J.C.; Singh, F.; Mishra, Y.; Avasthi, D.K.; Stoquert, J.P.*; Surf. & Coat. Tech.*, **2009**, *203*, 2432. **DOI:** 10.1016/j.surfcoat.2009.02.033
12. Avasthi, D.K.; Ghosh, S.; Srivastava, S.K.; Assmann, W.; *Nucl. Instr. and Meth. in Phys. Res. B.*, **2004**, *219–220*, 206. **DOI:** 10.1016/j.nimb.2004.01.055
13. Wang, Z.G.; Dufour, C.; Paumier, E.; Toulemonde, M.; *J. Phys.: Condens. Matter*; **1994**, *6*, 6733. **DOI:** 10.1088/0953-8984/7/12/015
14. Mohanty, T.; Satyam, P.V.; Mishra, N.C.; Kanjilal, D.; *Radiation Measurements*, **2003**, *36*, 137. **DOI:** 10.1016/S1350-4487(03)00110-0
15. Sinha, S.K.; Kothari, D.C; Balmuragan, A.K; Tyagi, A.K; Kanjilal. D.; *Surf. & Coat. Tech.*, **2002**, *158-159*, 214. **DOI:**10.1016/S0257-8972(02)00210-4
16. Gupta, A.; Meneghini, C.; Saraiya, A.; Principi, G.; Avasthi, D.K.; *Nucl. Instr. and Meth. In Phys. Res. B.*, **2003**, *212*, 458. **DOI:** 10.1016/S0168-583X(03)01725-7
17. Kumar, S.; Chauhan, R.S.; Khan, S.A.; Bolse, W.; Avasthi, D.K.; *Nucl. Instr. and Meth. in Phys. Res. B.*, **2006**, *244*, 194. **DOI:** 10.1016/j.nimb.2005.11.054
18. Jain, I.P.; Agarwal, G.; *Surface Science Reports*. **2011**, *66*, 77. **DOI:** 10.1016/j.surfrep.2010.11.001
19. Doolittle, L.R.; *Nucl. Instr. and Meth. in Phys. Res. B.*, **1985**, *9*, 344. **DOI:** 10.1016/0168-583X(85)90762-1
20. Toulemonde, M.; Trautmann, C.; Balanzat, E.; Hjort, K.; Weidinger, A.; *Nucl. Instr. and Meth. in Phys. Res. B.*, **2004**, *216*, 1. **DOI:** 10.1016/j.nimb.2003.11.013
21. Singh, U.B.; Agarwal, D.C.; Khan, S.A; Mohapatra, S.; Tripathi, A.; Avasthi, D.K.; *J. Phys. D: Appl. Phys*., **2012**, *45*, 445304. **DOI:** 10.1088/0022-3727/45/44/445304
22. Varma, R.S.; Kothari, D.C.; Choudhari, R.J.; Kumar, R.; Tewari, R.; Dey, G.K.; *Surf. Coat. & Tech.*, **2009**, *203*, 2468. **DOI:** 10.1016/j.surfcoat.2009.02.080
23. Sutherland, R.L.; 'Handbook of Nonlinear Optics', second ed. Dekker, New York, **2003**. **DOI:** isbn/9780824742430
24. Koushki, K.; Majles Ara, M.H.; Akherat Doost, H.; *Appl. Phys. B.*, **2014**, *115*, 279. **DOI:** 10.1007/s00340-013-5602-3.